# Two-species five-beam magneto-optical trap for erbium and dysprosium

P. Ilzhöfer,[1,2] G. Durastante,[1,2] A. Patscheider,[1,2] A. Trautmann,[2,*] M. J. Mark,[1,2] and F. Ferlaino[1,2,†]
[1]*Institut für Experimentalphysik und Zentrum für Quantenoptik, Universität Innsbruck, Technikerstrasse 25, 6020 Innsbruck, Austria*
[2]*Institut für Quantenoptik und Quanteninformation, Österreichische Akademie der Wissenschaften, 6020 Innsbruck, Austria*

(Received 20 November 2017; published 26 February 2018)

We report on the first realization of a two-species magneto-optical trap (MOT) for the highly magnetic erbium and dysprosium atoms. The MOT operates on an intercombination line for the respective species. Owing to the narrow-line character of such a cooling transition and the action of gravity, we demonstrate a trap geometry employing only five beams in the orthogonal configuration. We observe that the mixture is cooled and trapped very efficiently, with up to $5 \times 10^8$ Er atoms and $10^9$ Dy atoms at temperatures of about 10 $\mu$K. Our results offer an ideal starting condition for the creation of a dipolar quantum mixture of highly magnetic atoms.

DOI: 10.1103/PhysRevA.97.023633

Within the very active research field of ultracold quantum gases, heteronuclear mixtures of different atomic species offer unique possibilities to study a broad range of quantum phenomena. In the past 15 years, various atomic species have been combined to produce quantum degenerate mixtures. Each such quantum mixture has its own characteristic traits. Among the widely used alkali mixtures (e.g., [1,2]), the mass imbalance and the selective tuning of the intra- and interspecies interaction have allowed to investigate fascinating phenomena, such as heteronuclear Efimov states [3–6], polaron and impurity physics in both bosonic and fermionic backgrounds [7–11], and heteronuclear molecules with large electric dipole moments [12–14].

The latter development is mainly driven by the interest in studying phenomena arising from long-range and anisotropic dipole-dipole interactions among the molecules [15]. As an alternative approach, magnetic atoms have proven to be a robust system for study of few- and many-body dipolar physics. The strength of magnetic atoms for the study of dipolar physics was first shown using Bose-Einstein condensates of chromium atoms [16,17]. More recently, both erbium (Er) and dysprosium (Dy), among the most magnetic and isotope-rich atomic species, have been individually brought to quantum degeneracy [18–21]. Using these species, remarkable many-body dipolar phenomena have been observed, including the observation of deformed Fermi surfaces [22], quantum droplets [23–25], and roton excitations [26] and the recent study of thermalization in many-body dipolar gases [27].

Adding the flexibility of mixtures to the richness of magnetic atoms, we here report on the first combination of the two highly magnetic atomic species Er and Dy in a single experimental apparatus. The Er-Dy system extends the collection of available quantum mixtures by an unexplored case, as the interplay between the interspecies contact and dipolar interactions and the dipolar imbalance among the two species provides a new dimension in the parameter space of accessible quantum phenomena. This impacts, e.g., the miscibility properties of the mixture [28]. Although imbalanced dipolar mixture systems have not yet been considered in theory, they are good candidates for observation of, e.g., long-range dominated polarons, dipolar pairing, and the anisotropic BEC-BCS crossover with deformed Fermi surfaces.

While single-species magneto-optical traps (MOTs) of Er [29–31] and Dy [32–34] as well as other lanthanoid atoms [35–37] have already been attained, we simultaneously cool and trap Er and Dy in a two-species MOT operating on intercombination lines. We observe a remarkably robust operation of the dual MOT, with atom numbers similar or even surpassing the typical ones recorded in the single-species Er or Dy experiments. Moreover, we demonstrate magneto-optical trapping using a unique beam configuration, allowing us to efficiently operate the MOT using only five beams (5B) in an orthogonal *open-top* configuration; see Fig. 1(b). The working principle of our orthogonal 5B MOT relies on the combined effect of the narrow-line cooling and gravity [30,31,33–35,38] and contrasts with the classical six-beam (6B) approach.

A beneficial factor for combining the multivalence-electron atoms Er and Dy is their similarity in atomic properties [see table in Fig. 1(e)]. They both have several stable isotopes with a high natural abundance, >14%; in total, five bosonic ($^{166}$Er, $^{168}$Er, $^{170}$Er, $^{162}$Dy, $^{164}$Dy) and three fermionic ($^{167}$Er, $^{161}$Dy, $^{163}$Dy) isotopes. This isotope variety will allow us to prepare ultracold Bose-Bose, Bose-Fermi, and Fermi-Fermi quantum mixtures of Er and Dy. Whereas all bosonic isotopes have zero nuclear spin, the fermionic isotopes possess nuclear spins of $I_{\mathrm{Er}} = 7/2$ and $I_{\mathrm{Dy}} = 5/2$, leading to eight and six hyperfine states in the electronic ground state, respectively. Both elements exhibit a rich atomic energy spectrum, arising from their submerged-shell electronic configuration, featuring a [Xe] core, a partially filled inner $4f$ shell, and a closed outer $6s$ shell. The electron vacancy in the $4f$ shell is responsible for the large orbital quantum numbers and the respective high magnetic moments, i.e., $7\mu_B$ and $10\mu_B$ for Er and Dy, with $\mu_B$ being the Bohr magneton.

Figures 1(c) and 1(d) show the electronic levels of Er and Dy for wave numbers up to 26 000 cm$^{-1}$ [39]. While most of

*arno.trautmann@uibk.ac.at
†Corresponding author: Francesca.Ferlaino@uibk.ac.at

 

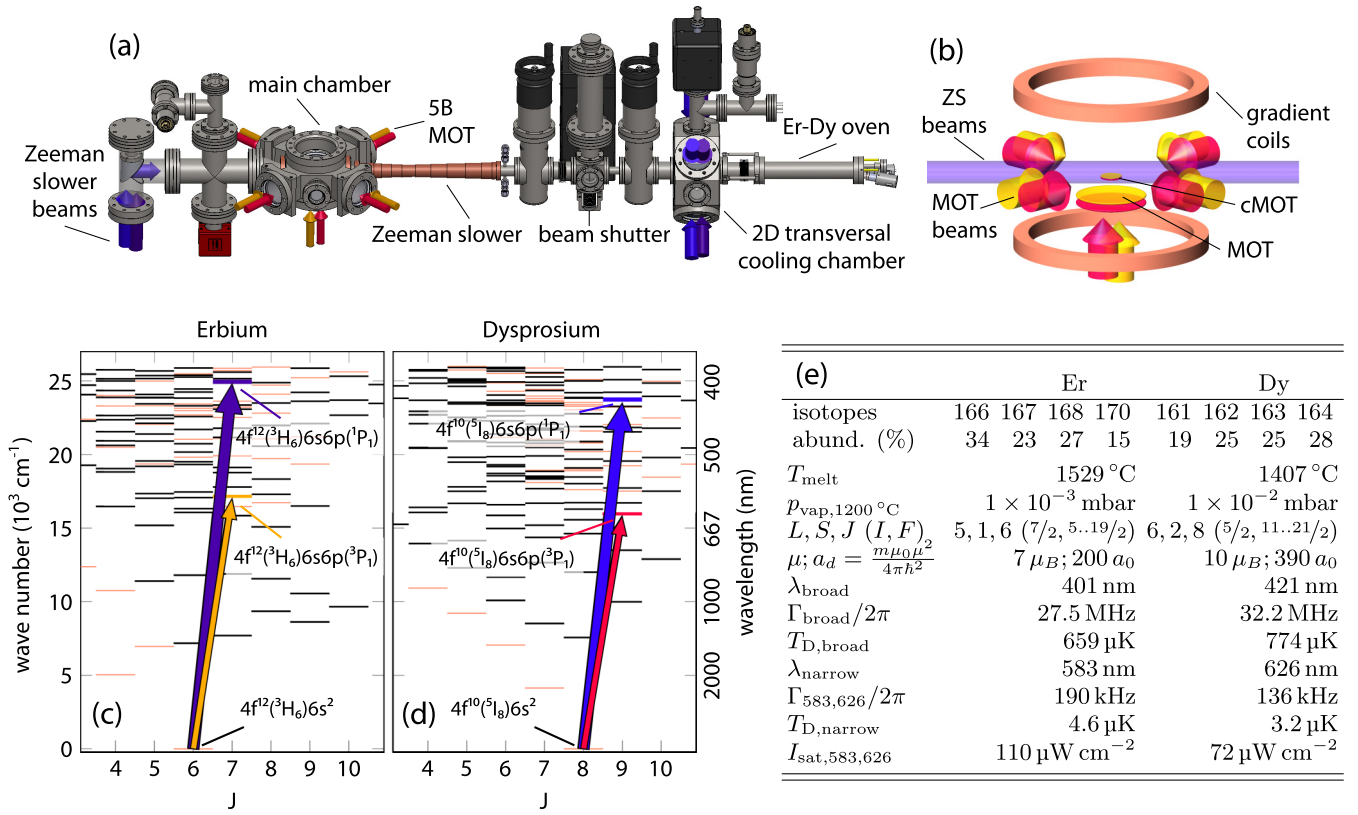


| (e) | Er | | | | Dy | | | |
|---|---|---|---|---|---|---|---|---|
| isotopes | 166 | 167 | 168 | 170 | 161 | 162 | 163 | 164 |
| abund. (%) | 34 | 23 | 27 | 15 | 19 | 25 | 25 | 28 |
| $T_{\mathrm{melt}}$ | 1529 °C | | | | 1407 °C | | | |
| $p_{\mathrm{vap,1200\,°C}}$ | $1\times10^{-3}$ mbar | | | | $1\times10^{-2}$ mbar | | | |
| $L,S,J\ (I,F)$ | $5,1,6\ (^7/_2,{}^{5..19}/_2)$ | | | | $6,2,8\ (^5/_2,{}^{11..21}/_2)$ | | | |
| $\mu;a_d=\frac{m\mu_0\mu^2}{4\pi\hbar^2}$ | $7\,\mu_B;200\,a_0$ | | | | $10\,\mu_B;390\,a_0$ | | | |
| $\lambda_{\mathrm{broad}}$ | 401 nm | | | | 421 nm | | | |
| $\Gamma_{\mathrm{broad}}/2\pi$ | 27.5 MHz | | | | 32.2 MHz | | | |
| $T_{\mathrm{D,broad}}$ | 659 µK | | | | 774 µK | | | |
| $\lambda_{\mathrm{narrow}}$ | 583 nm | | | | 626 nm | | | |
| $\Gamma_{583,626}/2\pi$ | 190 kHz | | | | 136 kHz | | | |
| $T_{\mathrm{D,narrow}}$ | 4.6 µK | | | | 3.2 µK | | | |
| $I_{\mathrm{sat},583,626}$ | 110 µW cm$^{-2}$ | | | | 72 µW cm$^{-2}$ | | | |

FIG. 1. Illustration of the vacuum apparatus, including the optical setup for the 5B MOT, and atomic properties of Er and Dy. (a) Er-Dy vacuum apparatus, including the high-temperature oven, transversal cooling chamber, Zeeman slower (ZS), and main chamber. The atomic beam propagates from right to left. The ZS beam is reflected by a metallic mirror in vacuum. (b) Sketch of the working principle of the open-top MOT. Arrows depict MOT beams, and the blue region indicates the ZS beam. For clarity, we depict the atomic clouds displaced from each other. (c, d) Energy level diagrams for Er and Dy up to 26 000 cm$^{-1}$ at different total electronic angular momentum quantum numbers $J$. States with odd (even) parity are indicated by black (orange) horizontal lines. Arrows show the broad and narrow laser-cooling transitions. (e) Table listing the atomic properties of Er and Dy.

the possible transitions are dipole forbidden, both species offer one particularly broad transition, suitable for laser cooling, to the respective singlet $6s6p$ state [blue arrows in Figs. 1(c) and 1(d)], which we label *broad* in the following. The blue transition light has a wavelength of 401 nm(421 nm), and the transition line width is $\Gamma_{\mathrm{broad}}/2\pi = 27.5$ MHz (32.2 MHz) for Er (Dy) [30,33]. We use this transition for transversal cooling, Zeeman slowing, and absorption imaging. The laser light, driving the broad transition, is derived from grating-stabilized laser diodes, followed by tapered amplifiers and frequency-doubling cavities. The laser systems emit more than 1W of power each. Both systems are frequency-stabilized using signals from modulation-transfer spectroscopy in hollow-cathode lamps [30].

Following previous single-species experiments with Yb [35], Er [30], and Dy [33,34], we produce the MOT using an intercombination line driving the transition from the ground state to the triplet $6s6p$ state [yellow (red) arrow in Figs. 1(c) and 1(d)] at a wavelength of 583 nm(626 nm) in Er (Dy) and a line width of $\Gamma_{583}/2\pi = 190$ kHz($\Gamma_{626}/2\pi = 136$ kHz). The narrow-width character of these transitions leads to the conveniently low Doppler temperatures of $T_{\mathrm{D,Er}} = 4.6\ \mu$K and $T_{\mathrm{D,Dy}} = 3.2\ \mu$K. The laser system for the Er MOT is based on a Raman fiber-amplified diode laser at 1166 nm and a single-pass frequency-doubling stage, with an output power above 1.7 W. The laser system for the Dy MOT is based on two fiber lasers operating at 1050 and 1550 nm, which are amplified and frequency-converted in a single-pass sum-generation stage, resulting in more than 1.6 W of output power. Both MOT laser systems are frequency-stabilized against long-term drifts on a home-built ultralow expansion cavity via a Pound-Drever-Hall lock [40] and have line widths below 100 kHz.

The experimental procedure generalizes our previously demonstrated single-species MOT approach [30] to two-species operation. The very similar strengths and wavelengths of the laser-cooling transitions of Er and Dy and their similar masses and melting points greatly simplify the design of the vacuum apparatus and the experimental procedure for the mixture. Figure 1(a) shows the experimental apparatus. Er and Dy atoms are emitted from a single high-temperature oven, consisting of two sections: The first section (effusion cell) operates at a temperature of 1100 °C, and the second one (hot lip) operates at 1200 °C, unless otherwise stated. Three apertures of different diameters, placed inside the oven, geometrically collimate the Er-Dy atomic beam before it enters the transversal-cooling chamber. We operate the transversal cooling resonantly on the broad transitions with total powers of 300 mW(120 mW) for Er (Dy) and elliptic waists of

approximately $w_{\text{horiz}} = 30$ mm and $w_{\text{vert}} = 6$ mm. We observe that the transversal cooling increases the MOT loading rate by a factor of 10 (6) for Er (Dy). The two-species atomic beam is slowed down to about 5 m/s using a two-species Zeeman slower (ZS) about 35 cm long in the spin-flip configuration. The magnetic-field values along the ZS are experimentally optimized for Dy and work equally well for Er. The two light beams for the ZS of Er and Dy are overlapped using dichroic optics and guided through the ZS via a metallic in-vacuum mirror [41]; see Fig. 1(a). The optimal performance of the ZS has been found for laser powers of 57 mW(121 mW) with beam waists of 4 mm at a detuning of −520 MHz(−530 MHz) for Er (Dy).

The slow atoms are then captured into a two-species MOT, operating on the respective intercombination line. Taking advantage of the similar wavelengths, we combine the MOT beams for both species into the same fibers. The MOT light is spectrally broadened utilizing electro-optic modulators with resonance frequencies of 139 kHz(102 kHz) for Er (Dy), which increases the capture range and thus the number of atoms in the MOT by a factor of 5 (2). The recapture volume is further enhanced by using large MOT beams, with diameters of about 36 mm. We observe an optimal loading for peak intensities of each laser beam of $I_{583} = 50 I_{\text{sat},583}$ and $I_{626} = 160 I_{\text{sat},626}$. Additionally, we endow our main chamber with inverted top and bottom view ports with large clear apertures of 64 mm. As discussed later, our special 5B MOT geometry allows us to completely free the top view, where we will implement a high-resolution *in situ* imaging with a numerical aperture of 0.45, which can resolve structures down to 600 nm. A pair of vertical coils creates a magnetic quadrupole field for the MOT of $\nabla B = 4.6$ G/cm. A vertical bias field of $B_0 = 2.9$ G shifts the zero point of the quadrupole field downwards. Additional coil pairs in the horizontal plane compensate for external magnetic fields.

We produce and study the Er-Dy MOT using two beam configurations. In the first one, we use a standard 6B geometry with three pairs of orthogonal retroreflected beams. For the second configuration, we remove the top → bottom MOT beam, demonstrating for the first time a 5B geometry with an open top; see Fig. 1(b). Although this 5B MOT would not work for alkali MOTs [42], we here demonstrate a very robust operation for our lanthanoid mixture. In the first set of experiments, we study the loading performance of our two-species MOT in both the 6B and the 5B configurations for $^{168}$Er and $^{164}$Dy. For all atom numbers we report in this paper, we load the MOTs at the optimized detuning for each setting as discussed later (see Fig. 3), apply a compression phase after MOT loading, and detect the atomic clouds using absorption imaging, as described later. Figure 2 shows the Er and Dy atom numbers as a function of the MOT loading time. From a fit to the data using a standard loading function, $N(t) = N_{\text{ss}}(1 - e^{-\gamma t})$, we extract the loading rate $R$ and decay rate $\gamma$ with the steady-state atom number $N_{\text{ss}} = R/\gamma$ (see Table I). In both the 6B and the 5B configurations, we observe a very efficient loading of the two-species MOT. After about 10 s of loading, the atom numbers approach their steady-state value of some $10^8$ atoms (see Table I). We do not observe any mutual influence of one species on the other, as reported for some alkaline mixtures, as, e.g., shown in Refs. [43] and [44].

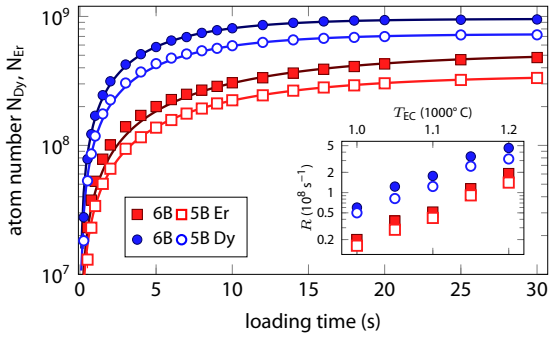


FIG. 2. Loading curve of the two-species MOT for the 6B and 5B configurations. Filled and open squares (circles) show data for the 6B and 5B Er (Dy) MOTs, respectively. The corresponding lines are fits to the data, as detailed in the text. Fit parameters are listed in Table I. Inset: Loading rate of the two species dependent on the effusion cell temperature $T_{\text{EC}}$. Note that the hot lip is always kept at $T_{\text{HL}} = T_{\text{EC}} + 100\,^{\circ}$C.

Given the complex scattering properties and optical spectra of multielectron lanthanoids, this surprising result enables the simultaneous MOT operation and greatly simplifies the experimental sequence.

The difference in the loading curves between Er and Dy is due to their different vapor pressures. The ratio of vapor pressures of Er and Dy is typically higher than 10 at the same temperature [45] and strongly temperature dependent, which would prevent an efficient simultaneous MOT loading. To mitigate this, we selectively heat up the atoms exploiting the two-section design of the oven. We fill the effusion cell with a 33%/67% alloy of Er/Dy and the hot-lip section with pure Er. We operate the oven with a differential temperature of 100 °C between the two sections. In the temperature range from 1000 °C to 1200 °C for the first section, we expect to reduce the vapor-pressure ratio among the two species to about 2.3. We investigate this effect by repeating the loading experiments for different temperatures of the effusion cell, while keeping the hot lip always 100 °C hotter; see Fig. 2 (inset). We observe a roughly constant loading ratio of between 2.5 and 3.5, which confirms the above expectations and shows that our concept of differential heating works very efficiently.

We remarkably find that the performance of the 5B MOT is only slightly below that of the 6B MOT. Moreover, even our 5B double-species MOT shows atom numbers similar to or larger than those previously reported for single-species Er or Dy MOT experiments [29,30,32–34]. Judging from our experience with

TABLE I. Loading rates $R$, decay rates $\gamma$, and steady-state atom numbers $N_{\text{ss}}$ obtained from fits to the data shown in Fig. 2. Values for both species in the 5B and 6B configurations are listed. Also listed are the lifetimes obtained from the data in Fig. 4.

| | Er | | Dy | |
|---|---|---|---|---|
| | 5B | 6B | 5B | 6B |
| $R$ ($10^8$ s$^{-1}$) | 0.35(1) | 0.45(2) | 1.21(4) | 1.79(3) |
| $\gamma$ (s$^{-1}$) | 0.100(2) | 0.086(6) | 0.166(7) | 0.187(5) |
| $N_{\text{ss}}$ ($10^8$) | 3.5(1) | 4.5(3) | 7.3(4) | 9.6(3) |
| Lifetime cMOT (ms) | 515(65) | 475(50) | 374(44) | 345(23) |

Er [30], we are thus confident that these numbers are sufficient for reaching quantum degeneracy. The 5B MOT configuration has the advantage of automatically spin-polarizing the atoms and providing full optical access through the vertical top view port, allowing implementation of optical setups which require large numerical apertures, e.g., high-resolution imaging or angle-resolved Bragg spectroscopy.

The simultaneous cooling and polarization of the intercombination MOT in lanthanoids has been studied for single-species Er [30] and Dy [34] 6B MOTs. In brief, the combined effects of a narrow-line MOT and gravity yield a peculiar semi-shell-shaped MOT with its center lying below the zero of the magnetic quadrupole field; see Fig. 1(b). The center position of the MOT can be adjusted by changing the MOT detuning. For large enough vertical displacement of the MOT, i. e., detuning, the atoms predominantly absorb $\sigma^-$-polarized photons, which are coming from the bottom-top beam. As a consequence, the atoms are spin-polarized into the lowest Zeeman sublevel. For lower detuning, the atoms can absorb both $\sigma^+$ and $\sigma^-$ light and the sample is unpolarized [34]. With our 5B MOT, we bring this concept to the extreme: We completely remove the ($\sigma^+$) top-bottom beam and force the atoms to sit only below the zero of the magnetic field. We verified the spin polarization by performing spin-resolved absorption imaging using the Stern-Gerlach technique. Within our experimental resolution, we do not detect atoms in higher Zeeman sublevels [46]. Thanks to this spontaneous spin polarization, optical-pumping schemes are not necessary. The spin purity is very beneficial for future loading of the mixture into an optical dipole trap, where the presence of additional spin states can lead to atomic losses via inelastic dipolar relaxation processes.

In the second set of experiments, we systematically study the effect of MOT-light detuning from the respective resonant atomic frequency on the atom number and compare the results for the 6B and 5B configurations after 5s of loading; see Fig. 3. For both species, we see a clear rise of atom numbers with increasing detuning. After reaching a maximum value the numbers undergo a sharp decrease at large detunings. This decrease can be simply explained by the spatial downshift of the MOT position with increasing detuning, eventually causing the atoms to leave the recapture volume. Here, the equal behavior of the 6B and 5B MOTs indicates that the top-bottom beam does not play a significant role. At intermediate detunings, however, the two configurations clearly show different behaviors. In particular, the 6B MOT has a much broader range of operation than the 5B configuration. We believe that this difference is due to the fact that the central cloud position approaches the magnetic-field zero point with decreasing detuning. In the absence of the top-bottom beam, atoms above the magnetic-field zero do not experience a restoring light force towards the trap center and may escape from the MOT. Contrariwise, in the 6B approach, these atoms are retrapped, resulting in the broader operation range in terms of detuning.

As observed in previous experiments [33], the Dy atom number shows a small dip at detunings around $-70\Gamma_{626\,\mathrm{nm}}$. We attribute this feature to a partial overlap of the cloud with the ZS light beam, which drives off-resonant pumping processes resulting in atom losses [30]. For Er, the influence of the ZS light is weaker due to its lower light intensity and larger relative detuning, and this effect is not observed.

Finally, we study the lifetime of the mixture in the compressed MOT (cMOT). The compression phase is essential to efficiently load an optical dipole trap in future experiments, as the compression reduces the temperature and increases the density of the mixture. After loading the MOT, we switch off the spectral broadening electro-optic modulators, the ZS beams, and block the atomic beam with a mechanical shutter. The compression has a duration of 200 ms, during which we (i) reduce the detuning of the MOT light to $10\,\Gamma_{583}$ ($18\,\Gamma_{626}$), (ii) decrease the MOT-beam power to $I_{583} = 0.17 I_{\mathrm{sat},583}$ and $I_{626} = 0.6 I_{\mathrm{sat},626}$, (iii) ramp down the magnetic-field gradient to $\nabla B = 4.3$ G cm$^{-1}$, and (iv) switch off the vertical bias magnetic field. As shown in Fig. 4, we observe that the double-species cMOT has a lifetime that is fully sufficient for loading of atoms into an optical dipole trap, which typically requires a holding time of about 100 ms. The data are taken in dual operation, with both species present in all settings. Again,

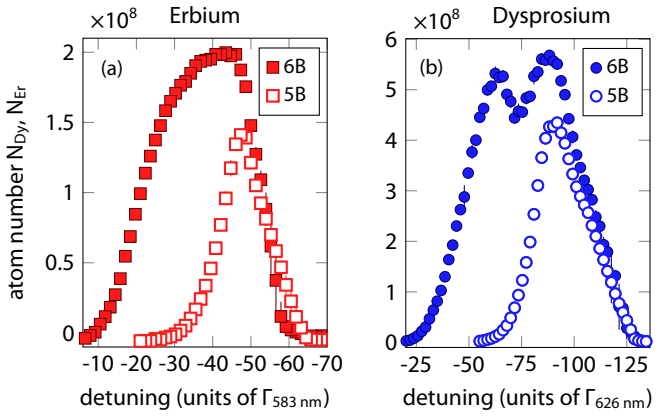


FIG. 3. Dependence of atom numbers in the cMOT on the initial MOT detuning, in units of the respective linewidth of the narrow transition of $\Gamma_{583}/2\pi = 190$ kHz($\Gamma_{626}/2\pi = 136$ kHz) for Er (Dy). Both species show broad ranges of detuning for efficient MOT loading in the 6B configuration, while 5B shows a narrower range. The optimal detunings are nearly equal for the 5B and 6B configurations. Data were taken for 5 s of MOT loading.

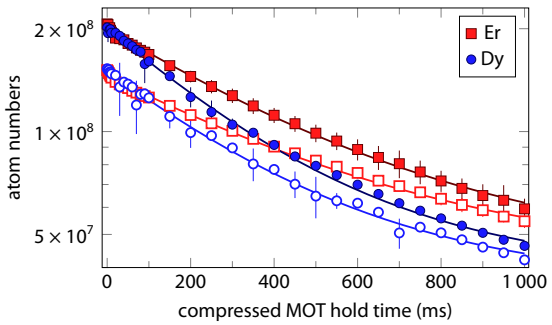


FIG. 4. Lifetime of the cMOT for both Er (red) and Dy (blue) in the 5B (open symbols) and 6B (filled symbols) configurations. We adjust the MOT loading time to compare samples with equal atom numbers. Solid lines show exponential fits to the respective data. From the fits we extract lifetimes of 515(65) and 475(5) ms [374(44) and 345(23) ms] for Er [Dy] in the 5B and 6B cMOTs, respectively.

we do not see any interplay between the species. The results of fits to the lifetime data are listed in Table I. Additionally, we extract temperatures of 11(1) $\mu$K [10(1) $\mu$K] for Er [Dy] in both the 5B and the 6B configurations from time-of-flight measurements. We observe that lower temperatures close to the Doppler temperatures can be achieved with different sets of parameters, at the expense of lower atom numbers. From our experience, we are certain that the observed lifetimes and temperatures are fully sufficient for efficient loading into an optical dipole trap as the next step towards quantum degeneracy.

The data we present here refer to the mixture of $^{168}$Er and $^{164}$Dy. Moreover, we are also able to trap and cool all other abundant bosonic isotopes with equally good performance, except for the $^{170}$Er MOT, which has smaller numbers, as expected from its low natural abundance. For future studies of the fermionic isotopes, no changes in the experimental apparatus are necessary.

In conclusion, we have demonstrated efficient cooling and trapping of an Er-Dy mixture in a two-species MOT operating on narrow-line transitions. In addition, we demonstrate a beam geometry for our two-species MOT which consists of only five laser beams in an open-top orthogonal setting. This geometry has the big advantage of providing free optical access from the top with a large numerical aperture, greatly simplifying the implementation, e.g., of high-resolution imaging, as well as optical lattices. Our recorded temperatures and atom numbers provide ideal conditions for subsequent evaporative cooling, towards the first production of a quantum-degenerate dipolar mixture. Optimization of the optical-trap loading and evaporative cooling is under way in our laboratory.

We acknowledge A. Frisch, T. Pyragius, and C. Zhang for support in the initial phase of the experiment. We thank the ERBIUM and the Dy-K teams in Innsbruck, the Er team at Harvard, and M. Sohmen and C. Politi for fruitful discussions. This work was supported by an ERC Consolidator Grant (RARE; No. 681432) and a FET Proactive Project (RySQ; No. 640378) of EU H2020. G.D. acknowledges support from the Austrian Science Fund FWF within DK-ALM: W1259-N27.

[1] Z. Hadzibabic, C. A. Stan, K. Dieckmann, S. Gupta, M. W. Zwierlein, A. Görlitz, and W. Ketterle, Phys. Rev. Lett. **88**, 160401 (2002).
[2] G. Roati, F. Riboli, G. Modugno, and M. Inguscio, Phys. Rev. Lett. **89**, 150403 (2002).
[3] G. Barontini, C. Weber, F. Rabatti, J. Catani, G. Thalhammer, M. Inguscio, and F. Minardi, Phys. Rev. Lett. **103**, 043201 (2009).
[4] R. Pires, J. Ulmanis, S. Häfner, M. Repp, A. Arias, E. D. Kuhnle, and M. Weidemüller, Phys. Rev. Lett. **112**, 250404 (2014).
[5] S.-K. Tung, K. Jiménez-García, J. Johansen, C. V. Parker, and C. Chin, Phys. Rev. Lett. **113**, 240402 (2014).
[6] L. J. Wacker, N. B. Jørgensen, D. Birkmose, N. Winter, M. Mikkelsen, J. Sherson, N. Zinner, and J. J. Arlt, Phys. Rev. Lett. **117**, 163201 (2016).
[7] A. Schirotzek, C.-H. Wu, A. Sommer, and M. W. Zwierlein, Phys. Rev. Lett. **102**, 230402 (2009).
[8] M. Koschorreck, D. Pertot, E. Vogt, B. Fröhlich, M. Feld, and M. Köhl, Nature **485**, 619 (2012).
[9] C. Kohstall, M. Zaccanti, M. Jag, A. Trenkwalder, P. Massignan, G. M. Bruun, F. Schreck, and R. Grimm, Nature **485**, 615 (2012).
[10] T. Rentrop, A. Trautmann, F. A. Olivares, F. Jendrzejewski, A. Komnik, and M. K. Oberthaler, Phys. Rev. X **6**, 041041 (2016).
[11] N. B. Jørgensen, L. Wacker, K. T. Skalmstang, M. M. Parish, J. Levinsen, R. S. Christensen, G. M. Bruun, and J. J. Arlt, Phys. Rev. Lett. **117**, 055302 (2016).
[12] K.-K. Ni, S. Ospelkaus, M. H. G. de Miranda, A. Pe'er, B. Neyenhuis, J. J. Zirbel, S. Kotochigova, P. S. Julienne, D. S. Jin, and J. Ye, Science **322**, 231 (2008).
[13] T. Takekoshi, L. Reichsöllner, A. Schindewolf, J. M. Hutson, C. R. Le Sueur, O. Dulieu, F. Ferlaino, R. Grimm, and H.-C. Nägerl, Phys. Rev. Lett. **113**, 205301 (2014).
[14] P. K. Molony, P. D. Gregory, Z. Ji, B. Lu, M. P. Köppinger, C. R. Le Sueur, C. L. Blackley, J. M. Hutson, and S. L. Cornish, Phys. Rev. Lett. **113**, 255301 (2014).
[15] G. Pupillo, A. Micheli, H. P. Büchler, and P. Zoller, in *Cold Molecules: Creation and Applications*, edited by R. V. Krems, B. Friedrich, and W. C. Stwalley (Taylor & Francis, London, 2004), pp. 266–290.
[16] A. Griesmaier, J. Werner, S. Hensler, J. Stuhler, and T. Pfau, Phys. Rev. Lett. **94**, 160401 (2005).
[17] Q. Beaufils, R. Chicireanu, T. Zanon, B. Laburthe-Tolra, E. Maréchal, L. Vernac, J.-C. Keller, and O. Gorceix, Phys. Rev. A **77**, 061601 (2008).
[18] M. Lu, N. Q. Burdick, S. H. Youn, and B. L. Lev, Phys. Rev. Lett. **107**, 190401 (2011).
[19] M. Lu, N. Q. Burdick, and B. L. Lev, Phys. Rev. Lett. **108**, 215301 (2012).
[20] K. Aikawa, A. Frisch, M. Mark, S. Baier, A. Rietzler, R. Grimm, and F. Ferlaino, Phys. Rev. Lett. **108**, 210401 (2012).
[21] K. Aikawa, A. Frisch, M. Mark, S. Baier, R. Grimm, and F. Ferlaino, Phys. Rev. Lett. **112**, 010404 (2014).
[22] K. Aikawa, S. Baier, A. Frisch, M. Mark, C. Ravensbergen, and F. Ferlaino, Science **345**, 1484 (2014).
[23] H. Kadau, M. Schmitt, M. Wenzel, C. Wink, T. Maier, I. Ferrier-Barbut, and T. Pfau, Nature **530**, 194 (2016).
[24] M. Schmitt, M. Wenzel, F. Böttcher, I. Ferrier-Barbut, and T. Pfau, Nature **539**, 259 (2016).
[25] L. Chomaz, S. Baier, D. Petter, M. J. Mark, F. Wächtler, L. Santos, and F. Ferlaino, Phys. Rev. X **6**, 041039 (2016).
[26] L. Chomaz, R. M. W. van Bijnen, D. Petter, G. Faraoni, S. Baier, J. H. Becher, M. J. Mark, F. Waechtler, L. Santos, and F. Ferlaino, arXiv:1705.06914.
[27] Y. Tang, W. Kao, K.-Y. Li, S. Seo, K. Mallayya, M. Rigol, S. Gopalakrishnan, and B. L. Lev, arXiv:1707.07031.
[28] R. K. Kumar, P. Muruganandam, L. Tomio, and A. Gammal, J. Phys. Commun. **1**, 035012 (2017).
[29] A. J. Berglund, S. A. Lee, and J. J. McClelland, Phys. Rev. A **76**, 053418 (2007).
[30] A. Frisch, K. Aikawa, M. Mark, A. Rietzler, J. Schindler, E. Zupanič, R. Grimm, and F. Ferlaino, Phys. Rev. A **85**, 051401 (2012).

[31] J. Ulitzsch, D. Babik, R. Roell, and M. Weitz, Phys. Rev. A **95**, 043614 (2017).
[32] M. Lu, S. H. Youn, and B. L. Lev, Phys. Rev. Lett. **104**, 063001 (2010).
[33] T. Maier, H. Kadau, M. Schmitt, A. Griesmaier, and T. Pfau, Opt. Lett. **39**, 3138 (2014).
[34] D. Dreon, L. A. Sidorenkov, C. Bouazza, W. Maineult, J. Dalibard, and S. Nascimbene, J. Phys. B **50**, 065005 (2017).
[35] T. Kuwamoto, K. Honda, Y. Takahashi, and T. Yabuzaki, Phys. Rev. A **60**, R745(R) (1999).
[36] D. Sukachev, A. Sokolov, K. Chebakov, A. Akimov, S. Kanorsky, N. Kolachevsky, and V. Sorokin, Phys. Rev. A **82**, 011405 (2010).
[37] J. Miao, J. Hostetter, G. Stratis, and M. Saffman, Phys. Rev. A **89**, 041401 (2014).
[38] H. Katori, T. Ido, Y. Isoya, and M. Kuwata-Gonokami, Phys. Rev. Lett. **82**, 1116 (1999).
[39] A. Kramida, Yu. Ralchenko, J. Reader, and NIST ASD Team, *NIST Atomic Spectra Database (version 5)* [online]. Available at: http://physics.nist.gov/asd. Accessed: 13 February 2018.
[40] R. W. P. Drever, J. L. Hall, F. V. Kowalski, J. Hough, G. M. Ford, A. J. Munley, and H. Ward, Appl. Phys. B **31**, 97 (1983).
[41] The atomic beam of Er and Dy might deposit an additional metallic layer on the mirror. However, we have tested this effect in our running Er machine and did not observe any sizable reduction in the reflectivity of the mirror.
[42] For the sake of completeness, we note that early MOT experiments on alkali atoms have explored MOT geometries with five non–orthogonally intersecting beams (e.g., at an angle of 120°) [47,48], which constitutes a very different scenario compared to our open-top approach.
[43] U. Schlöder, H. Engler, U. Schünemann, R. Grimm, and M. Weidemüller, Eur. Phys. J. D **7**, 331 (1999).
[44] M. Taglieber, A.-C. Voigt, F. Henkel, S. Fray, T. W. Hänsch, and K. Dieckmann, Phys. Rev. A **73**, 011402 (2006).
[45] C. E. Habermann and A. H. Daane, J. Chem. Phys. **41**, 2818 (1964).
[46] Since the large spatial extension of the MOT might mask residual atoms in higher spin states, we performed preliminary Stern-Gerlach mapping after loading the atoms into an optical dipole trap. Again, we did not detect atoms in higher Zeeman sublevels.
[47] J. Arlt, P. Bance, S. Hopkins, J. Martin, S. Webster, A. Wilson, K. Zetie, and C. J. Foot, J. Phys. B **31**, L321 (1998).
[48] A. di Stefano, D. Wilkowski, J. Müller, and E. Arimondo, Appl. Phys. B **69**, 263 (1999).